B-spline *R*-matrix-with-pseudostates calculations for electron-impact excitation and ionization of fluorine

Viktor Gedeon, Sergej Gedeon, Vladimir Lazur, and Elizabeth Nagy
Department of Theoretical Physics, Uzhgorod State University, Uzhgorod 88000, Ukraine

Oleg Zatsarinny* and Klaus Bartschat†
Department of Physics and Astronomy, Drake University, Des Moines, Iowa 50311, USA
(Received 19 March 2014; published 19 May 2014)

The *B*-spline *R*-matrix method is used to study electron collisions with neutral fluorine over an energy range from threshold to 100 eV. The multiconfiguration Hartree-Fock method in connection with *B*-spline expansions is employed for an accurate representation of the target wave functions. The sensitivity of the results is checked by comparing data obtained in different approximations, including a large-scale model with over 600 continuum pseudostates. Both correlation and polarization effects are found to be important for accurate calculations of the cross sections. Coupling to the target continuum strongly affects transitions from the ground state, but to a lesser extent the strong transitions between excited states. Cross sections are presented for selected transitions between the lowest 26 states of fluorine, as well as elastic scattering from and ionization of the ground state. The current predictions represent an extensive set of electron scattering data for neutral fluorine.

DOI: 10.1103/PhysRevA.89.052713 PACS number(s): 34.80.Bm, 34.80.Dp

I. INTRODUCTION

Electron-impact cross sections of fluorine gases are needed as input data for calculations of the chemical and electrical properties of processing plasmas and rare-gas-fluorine lasers. Many plasma processes use fluorine atoms as the dominant etching species. Fluorine is among the most reactive elements, and its high chemical activity makes it difficult to obtain reliable values of the electron-impact cross sections from direct measurements. Of the available cross sections on atomic fluorine only ionization has been determined experimentally. For modeling applications, the elastic, momentum-transfer, and electron excitation cross sections must be taken from theoretical estimates. Atomic cross sections can also be used to predict cross sections for different fluorine compounds.

The cross section for elastic scattering by atomic fluorine was calculated many decades ago by Robinson and Geltman [1], for electron energies up to 10 eV. These authors used a central-field model for the bound and continuum states, in which a model potential was adjusted to yield the observed binding energies of the negative ion. Their elastic cross section exhibits a smooth energy dependence. Later Ormonde [2] used the close-coupling (CC) method and reported very narrow ^1P and ^1D d-wave shape resonances in e–F scattering, very close to the elastic threshold. These resonances, if confirmed, would lead to very large near-threshold values of the electron- and photodetachment cross sections of F^- and could possibly affect the energy deposition rates in electron-beam-pumped H_2/F_2 and rare-gas/F_2 mixtures. When these close-coupling calculations were later repeated by Robb and Henry [3] using an independent CC computer program, no evidence for low-energy shape resonances was observed. This conclusion was confirmed by Rescigno *et al.* [4] in their calculations with model polarization potentials. No angle-integrated elastic cross sections were reported in these works.

To our knowledge, the only calculation of excitation cross sections for electron scattering from atomic fluorine was reported by Baliyan and Bhatia [5]. They used the standard Belfast *R*-matrix method [6] and presented collision strengths for all transitions between the lowest 11 states of neutral fluorine, at incident electron energies up to 40 eV. The authors expected their results to be of high accuracy in the energy range considered, but that they might be affected at higher energies when more target states should be included in the CC expansion.

The electron-impact ionization cross section for atomic fluorine was measured by Hayes *et al.* [7] from threshold to 200 eV. The absolute accuracy of the data was estimated as ±20%. To our knowledge, no calculations for fluorine ionization have been reported in the literature.

The purpose of the present paper is to provide an extensive and complete (for most modeling applications) set of electron scattering data for neutral fluorine, including elastic scattering, momentum-transfer, excitation, and ionization from the ground state. The calculations reported below were carried out with our highly sophisticated *B*-spline *R*-matrix (close-coupling) code [8]. The distinct feature of the approach is its ability to employ term-dependent nonorthogonal orbitals in the description of the target states. This allows us to optimize individual atomic wave functions independently and thereby generate a more accurate description of the target states than what is usually possible when orthogonality restrictions are imposed. Over the past decade, the BSR code (along with its fully relativistic extension, DBSR [9]) has been successfully applied to a number of targets [10], and in many cases the cross sections are more accurate than what was obtained using the standard *R*-matrix technique. Note that the BSR suite of programs forms a general code for many-electron targets. Its advantages are particularly seen in cases of electron scattering from systems with complex configurational structure, including multiple open shells. Examples include

*oleg.zatsarinny@drake.edu
†klaus.bartschat@drake.edu

electron scattering from the open-shell atoms O [11], S [12], and Cl [13], of which the latter has a similar electronic valence structure to the atomic fluorine that we are interested in here.

This manuscript is organized as follows: After discussing the description of the target structure, we summarize the most important aspects of the collision calculations. This is followed by a presentation of the cross sections for the most important transitions, starting with elastic scattering from F in its ground state. Due to the lack of experimental results available for comparison, we present two sets of calculations, with 39 and 690 target states, respectively, included in the close-coupling expansion. The first model only contains physical bound states, while the second one also includes continuum pseudostates. Comparison of the results from these two calculations provides some indication about the sensitivity of the predicted cross sections to the details of the model.

II. COMPUTATIONAL DETAILS

A. Structure calculations

The target states of fluorine in the present calculations were generated by combining the multiconfiguration Hartree-Fock (MCHF) and the B-spline box-based close-coupling methods [14]. We tried to account for the principal correlation effects, while bearing in mind that the final multiconfiguration expansions still need to be dealt with in the subsequent collision calculation with one more electron to be coupled in. Since relativistic effects are relatively small in fluorine, we used the nonrelativistic LS-coupling approximation, with the structure of the multichannel target expansion chosen as

$$\Phi(2s^2 2p^4 nl, LS) = \sum_{nl, L'S'} \left\{\phi(2s^2 2p^4, L'S')P(nl)\right\}^{LS} + \sum_{nl, L'S'} \left\{\phi(2s2p^5, L'S')P(nl)\right\}^{LS} + a\varphi(2s^2 2p^5)^2 P + b\varphi(2s2p^6)^2 S. \quad (1)$$

Here $P(nl)$ denotes the wave function of the outer valence electron, while the ϕ and φ functions stand for the configuration interaction (CI) expansions of the corresponding ionic and specific atomic states, respectively. These expansions were generated in separate MCHF calculations for each state using the MCHF program [15]. The expansion (1) can be considered as a model for the entire $2s^2 2p^4 nl$ and $2s2p^5 nl$ Rydberg series of the fluorine spectrum, including autoionizing states and continuum pseudostates. Inner-core (short-range) correlation is included through the CI expansion of the ionic states. These expansions include all single and double excitations from the $2s$ and $2p$ orbitals to the $4l$ and $5l$ ($l = 0$–4) correlated orbitals, again obtained from separate MCHF calculations. The core-valence correlation is partly included for the $2s^2 2p^4 nl$ states due to the presence of the $2s2p^5$ ionic states. This corresponds to the inclusion of correlation configurations with the important $2s \rightarrow 2p$ promotion. A more extensive description of core-valence correlation would require additional ionic states, such as $2s^2 2p^3 3s$ or $2s^2 2p^3 3d$, to describe important $2p \rightarrow 3s$ and $2p \rightarrow 3d$ transitions. Their inclusion, however, would have considerably increased the target expansions and made them no longer tractable in the subsequent scattering calculations. In order to keep the final expansions for the atomic states to a reasonable size, all ionic contributions with expansion coefficients of magnitude less than 0.01 were neglected.

The unknown functions $P(nl)$ for the outer valence electron were expanded in a B-spline basis, and the corresponding equations were solved subject to the condition that the wave functions vanish at the boundary. The B-spline coefficients for the valence orbitals $P(nl)$, along with the coefficients a and b, were obtained by diagonalizing the N-electron atomic Hamiltonian. Since the B-spline bound-state close-coupling calculations generate different nonorthogonal sets of orbitals for each atomic state, their subsequent use is somewhat complicated. On the other hand, our configuration expansions for the atomic target states contained from 100 to 500 configurations for each state and hence could be used in the collision calculations with the available computational resources.

TABLE I. Binding energies (in eV) for the spectroscopic target states included in our CC expansion.

	State	Term	Present	NIST [16]	Diff.
1	$2p^5$	$^2P^o$	−17.367	−17.406	0.039
2	$2p^4(^3P)3s$	^4P	−4.549	−4.706	0.157
3	$2p^4(^3P)3s$	^2P	−4.275	−4.424	0.149
4	$2p^4(^3P)3p$	$^4P^o$	−2.985	−3.041	0.056
5	$2p^4(^3P)3p$	$^4D^o$	−2.848	−2.899	0.051
6	$2p^4(^3P)3p$	$^2D^o$	−2.783	−2.827	0.044
7	$2p^4(^3P)3p$	$^2S^o$	−2.697	−2.742	0.045
8	$2p^4(^3P)3p$	$^4S^o$	−2.694	−2.740	0.046
9	$2p^4(^3P)3p$	$^2P^o$	−2.639	−2.671	0.032
10	$2p^4(^1D)3s$	^2D	−1.871	−2.059	0.188
11	$2p^4(^3P)4s$	^4P	−1.807	−1.827	0.020
12	$2p^4(^3P)4s$	^2P	−1.739	−1.753	0.014
13	$2p^4(^3P)3d$	^4D	−1.540	−1.541	0.001
14	$2p^4(^3P)3d$	^2D	−1.531	−1.532	0.001
15	$2p^4(^3P)3d$	^4F	−1.515	−1.500	−0.015
16	$2p^4(^3P)3d$	^2F	−1.514	−1.500	−0.014
17	$2p^4(^3P)3d$	^4P	−1.501	−1.487	−0.014
18	$2p^4(^3P)3d$	^2P	−1.499	−1.472	−0.027
19	$2p^4(^3P)4p$	$^4P^o$	−1.366	−1.373	0.007
20	$2p^4(^3P)4p$	$^4D^o$	−1.326	−1.331	0.005
21	$2p^4(^3P)4p$	$^2D^o$	−1.304	−1.297	−0.007
22	$2p^4(^3P)4p$	$^2S^o$	−1.281	−1.286	0.005
23	$2p^4(^3P)4p$	$^4S^o$	−1.280	−1.277	−0.003
24	$2p^4(^3P)4p$	$^2P^o$	−1.268	−1.254	−0.014
25	$2p^4(^3P)5s$	^4P	−0.968	−0.968	0.000
26	$2p^4(^3P)5s$	^2P	−0.941	−0.924	−0.017
27	$2p^4(^1D)3p$	$^2F^o$	−0.287		
28	$2p^4(^1D)3p$	$^2P^o$	−0.235		
29	$2p^4(^1D)3p$	$^2D^o$	−0.156	−0.226	0.070
30	$2p^4(^1D)4s$	^2D	0.802	0.762	0.040
31	$2p^4(^1S)3s$	^2S	0.955	0.791	0.164
32	$2p^4(^1D)3d$	^2P	1.055	1.043	0.012
33	$2p^4(^1D)3d$	^2G	1.059	1.047	0.012
34	$2p^4(^1D)3d$	^2D	1.078	1.066	0.012
35	$2p^4(^1D)3d$	^2F	1.088	1.076	0.012
36	$2p^4(^1S)3s$	^2S	1.100	1.074	0.026
37	$2p^4(^1S)3p$	$^2P^o$	2.747		
38	$2p^4(^1S)4s$	^2S	3.692		
39	$2p^4(^1S)3d$	^2D	4.057		

The number of spectroscopic bound states that can be generated in the above scheme depends on the B-spline box radius. In the present calculations, this radius was set to $30\,a_0$, where $a_0 = 0.529 \times 10^{-10}$ m is the Bohr radius. That allowed us to obtain good descriptions of the fluorine states with principal quantum number for the valence electron up to $n = 5$.

Table I compares the calculated spectrum of fluorine with the experimental values [16] for various multiplets included in the scattering calculations (see below). The overall agreement between experiment and theory is very satisfactory, with the deviation in the energy splitting being less than 0.05 eV for most of the states. Larger deviations of up to ≈0.2 eV are observed only for the $2p^4 3s$ states. This is expected due the core-valence correlation, which could not be included in our target expansions to sufficient extent, as discussed above.

The quality of our target description can be further assessed by comparing the results for the oscillator strengths of various transitions with experimental data and other theoretical predictions. Accurate oscillator strengths are very important to obtain reliable absolute values for the excitation cross sections, especially for optically allowed transitions at high electron energies. A comparison of our oscillator strengths is given in Table II with the most recent large-scale MCHF calculations of Froese Fischer and Tachiev [17] and the experimental data from the NIST compilation [16]. The experimental gf values for the fine-structure transitions were converted to the multiplet LS values. Experimental data are only available for a few transitions between the $3s$ and $3p$ levels, and we see good agreement with experiment for all these transitions. Overall, there is close agreement with the MCHF results [17] for most transitions, with noticeable differences only for weak transitions with gf values less than 0.1. Table II also contains the ratio of theoretical oscillator strengths obtained in the length and velocity forms of the electric dipole operator. This ratio can, to some extent, be considered an accuracy indicator for the calculated f-values. For most transitions, the length (f_L) and velocity (f_V) values agree within a few percent, in both the BSR and MCHF calculations.

TABLE II. Comparison of weighted oscillator strengths in F.

Lower level	Upper level	Present		MCHF		NIST
		gf_L	f_L/f_V	gf_L	f_L/f_V	
$2p^5\,{}^2P^o$	$2p^4 3s\,{}^2P$	0.559	1.00	0.586	1.00	
	$2p^4 3s\,{}^2D$	0.286	0.98	0.306	0.99	
	$2p^4 4s\,{}^2P$	0.106	1.01	0.585	1.01	
	$2p^4 3d\,{}^2D$	0.125	1.08	0.150	1.28	
	$2p^4 3d\,{}^2P$	0.028	1.12	0.041	1.28	
	$2p^4 5s\,{}^2P$	0.039	1.00			
$2p^4 3s\,{}^4P$	$2p^4 3p\,{}^4P^o$	3.815	1.12	3.834	1.03	3.48
	$2p^4 3p\,{}^4D^o$	6.637	0.96	6.734	1.10	6.36
	$2p^4 3p\,{}^4S^o$	1.337	1.20	1.420	1.16	1.32
	$2p^4 4p\,{}^4D^o$	0.056	0.89			
$2p^4 3s\,{}^2P$	$2p^4 3p\,{}^2D^o$	3.303	0.97	3.166	0.97	3.18
	$2p^4 3p\,{}^2S^o$	0.662	1.16	0.661	1.04	0.66
	$2p^4 3p\,{}^2P^o$	2.158	1.02	2.060	0.92	2.04
	$2p^4 4p\,{}^2P^o$	0.030	1.07			
$2p^4 3p\,{}^4P^o$	$2p^4 4s\,{}^4P$	1.691	1.06			
	$2p^4 3d\,{}^4D$	8.032	0.99	8.954	1.18	
	$2p^4 3d\,{}^4P$	2.675	1.05	2.935	1.16	
	$2p^4 5s\,{}^4P$	0.193	1.08			
$2p^4 3p\,{}^4D^o$	$2p^4 4s\,{}^4P$	3.453	1.00			
	$2p^4 3d\,{}^4D$	2.794	1.05	2.844	1.04	
	$2p^4 3d\,{}^4F$	15.42	0.97	16.15	1.26	
	$2p^4 3d\,{}^4P$	0.147	1.12	0.230	1.56	
	$2p^4 5s\,{}^4P$	0.315	1.01			
$2p^4 3p\,{}^2D^o$	$2p^4 4s\,{}^2P$	1.662	1.00			
	$2p^4 3d\,{}^2D$	1.421	1.04	1.388	0.97	
	$2p^4 3d\,{}^2F$	7.875	0.96	7.859	1.03	
	$2p^4 3d\,{}^2P$	0.081	1.09	0.107	1.51	
	$2p^4 5s\,{}^2P$	0.167	1.01			
$2p^4 3p\,{}^4S^o$	$2p^4 4s\,{}^4P$	0.846	1.09			
	$2p^4 3d\,{}^4P$	3.725	1.01	3.645	0.95	
	$2p^4 5s\,{}^4P$	0.053	1.15			
$2p^4 3p\,{}^2S^o$	$2p^4 4s\,{}^2P$	0.379	1.06			
	$2p^4 3d\,{}^2P$	1.880	1.02	1.809	0.94	
	$2p^4 5s\,{}^2P$	0.032	1.10			
$2p^4 3p\,{}^2P^o$	$2p^4 3s\,{}^2D$	0.023	0.42	0.009	2.25	
	$2p^4 4s\,{}^2P$	1.121	0.98			
	$2p^4 3d\,{}^2D$	4.282	1.00	3.751	0.86	
	$2p^4 3d\,{}^2P$	1.465	1.05	1.255	0.85	
	$2p^4 5s\,{}^2P$	0.096	0.97			
$2p^4 4s\,{}^4P$	$2p^4 4p\,{}^4P^o$	5.538	1.05			
	$2p^4 4p\,{}^4D^o$	9.831	0.98			
	$2p^4 4p\,{}^4S^o$	2.061	1.07			
$2p^4 4s\,{}^2P$	$2p^4 4p\,{}^2D^o$	4.889	0.99			
	$2p^4 4p\,{}^2S^o$	1.015	1.06			
	$2p^4 4p\,{}^2P^o$	2.945	1.01			
$2p^4 3d\,{}^4D$	$2p^4 4p\,{}^4P^o$	2.087	0.98			
	$2p^4 4p\,{}^4D^o$	0.802	1.01			
$2p^4 3d\,{}^2D$	$2p^4 4p\,{}^2D^o$	0.422	1.00			
	$2p^4 4p\,{}^2P^o$	1.324	1.01			
$2p^4 3d\,{}^4F$	$2p^4 4p\,{}^4D^o$	4.267	0.97			
$2p^4 3d\,{}^2F$	$2p^4 4p\,{}^2D^o$	2.285	0.95			
$2p^4 3d\,{}^4P$	$2p^4 4p\,{}^4P^o$	0.685	1.02			
	$2p^4 4p\,{}^4D^o$	0.020	1.11			
	$2p^4 4p\,{}^4S^o$	1.053	0.98			
$2p^4 3d\,{}^2P$	$2p^4 4p\,{}^2D^o$	0.016	1.00			
	$2p^4 4p\,{}^2S^o$	0.544	0.99			
	$2p^4 4p\,{}^2P^o$	0.467	1.04			

B. Collision calculations

The close-coupling expansion in our most extensive model includes 690 states of neutral fluorine, with 53 states representing the bound spectrum and the remaining 637 the target continuum corresponding to ionization of the $2p$ and $2s$ subshells. We included all doublet and quartet target states of configurations $2s^2 2p^4 nl$ and $2s 2p^5 nl$ with orbital angular momentum $l = 0$–3 for the outer electron and the total orbital angular momentum $L = 0$–5. The continuum pseudostates in the present calculations cover the energy region up to 20 eV above the ionization limit. This model will be referred to as BSR-690 below. As a check for the sensitivity of the results regarding coupling to the high-lying Rydberg states as well as the ionization continuum, we also performed a 39-state calculation (labeled BSR-39) with the spectroscopic target states listed in Table I. These states have the same target expansions as those in the BSR-690 model.

The close-coupling equations were solved by means of the R-matrix method, using a parallelized version of the BSR code [8]. The distinctive feature of the method is the use of B-splines

TABLE II. (*Continued.*)

Lower level	Upper level	Present		MCHF		NIST
		gf_L	f_L/f_V	gf_L	f_L/f_V	
$2p^4 4p\ ^4P^o$	$2p^4 5s\ ^4P$	3.101	1.03			
$2p^4 4p\ ^4D^o$	$2p^4 5s\ ^4P$	6.310	1.00			
$2p^4 4p\ ^2D^o$	$2p^4 5s\ ^2P$	3.045	1.00			
$2p^4 4p\ ^4S^o$	$2p^4 5s\ ^4P$	1.560	1.04			
$2p^4 4p\ ^2S^o$	$2p^4 5s\ ^2P$	0.703	1.03			
$2p^4 4p\ ^2P^o$	$2p^4 5s\ ^2P$	1.850	1.00			

as a universal basis to represent the scattering orbitals in the inner region of $r \leqslant a$. Hence the R-matrix expansion in this region takes the form

$$\Psi_k(x_1,\ldots,x_{N+1}) = \mathcal{A}\sum_{ij}\bar{\Phi}_i(x_1,\ldots,x_N;\hat{\mathbf{r}}_{N+1}\sigma_{N+1})r_{N+1}^{-1}B_j(r_{N+1})\,a_{ijk} + \sum_i \chi_i(x_1,\ldots,x_{N+1})\,b_{ik}. \quad (2)$$

Here the $\bar{\Phi}_i$ denote the channel functions constructed from the N-electron target states, while the splines $B_j(r)$ represent the continuum orbitals. The χ_i are additional $(N+1)$-electron bound states. In standard R-matrix calculations [6], the latter are included one configuration at a time to ensure completeness of the total trial wave function and to compensate for orthogonality constraints imposed on the continuum orbitals. The use of nonorthogonal one-electron radial functions in the BSR method, on the other hand, allows us to completely avoid these configurations for compensating orthogonality restrictions. This procedure has practical advantages in reducing pseudoresonance structure in the scattering solutions (see, for example, the discussion in Ref. [18]). We also note that Gorczyca and Badnell [19] suggested a practical method to address the problem in the standard R-matrix framework.

Usually, the bound channels in the BSR calculations are used for a more accurate description of the true bound states in the collision system, e.g., the $(2s^2 2p^6)^1S$ bound state of the F^- negative ion. In the present calculations we did not employ any $(N+1)$-electron correlation configurations in the expansion (2). Using just the pure close-coupling expansion, we obtained a fluorine electron affinity of -3.254 eV. This is close to the experimental value of -3.401 eV [20], indicating that our target expansions contain the main correlation corrections.

The B-spline basis in the present calculations contains 68 splines of order 8, with the maximum interval in this grid of $0.65a_0$. This is sufficient for a good representation of the scattering electron wave functions for energies up to 150 eV. The BSR-690 collision model contained up to 1727 scattering channels, leading to generalized eigenvalue problems with matrix dimensions up to 100 000 in the B-spline basis. Direct numerical calculations were performed for partial waves with total orbital angular momenta $L \leqslant 25$. Taking into account the total spin and parity leads to 156 partial waves overall. A top-up procedure based on the geometric-series approximation was used to estimate the contribution from higher L values if needed. The calculation for the external region was performed using a parallelized version of the STGF program [21].

III. RESULTS

Results for the elastic cross sections for electron scattering from the ground state of fluorine are presented in Fig. 1, where we compare the present results from the BSR-39 and BSR-690 models with the semiempirical calculations by Robinson and Geltman [1]. Except for two very narrow structures between 12 and 15 eV, all calculations predict a similar, smooth energy dependence with a maximum around 10 eV. Including the continuum pseudostates in BSR-690 model decreases the maximum by about 15% in comparison to the BSR-39 calculations. The BSR-690 cross sections regularly exceed the results from the model-potential calculations [1], with overall good agreement in the energy dependence. The present elastic cross sections are finite at threshold. The BSR-690 scattering lengths are 0.487 and 0.212 for the $^1P^o$ and $^3P^o$ partial waves, respectively. They drastically differ from the scattering lengths for electron scattering from chlorine [13]. The outer-shell configuration ground state of chlorine, $3p^5$, is similar to that of the fluorine ground state, $2p^5$, and hence one might expect similar results. However, the chlorine scattering lengths are negative and the elastic cross section exhibits a Ramsauer minimum near threshold, whereas the fluorine scattering lengths are positive and the elastic cross section decreases smoothly towards the threshold.

Cross sections as a function of energy for the most important transitions from the ground state and between the excited states are presented in Figs. 2–4, for dipole, nondipole, and exchange transitions, respectively. All electron energies are given relative to the ground state. Due to the almost complete absence of other theoretical results and experimental data, we compare our predictions from two sets of calculations, BSR-690 and BSR-39, which differ by including the

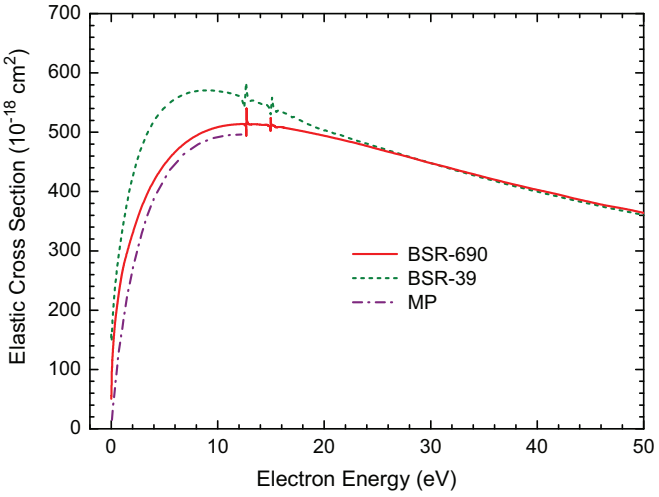

FIG. 1. (Color online) Cross sections for elastic electron scattering from fluorine atoms in their $(2p^5)^2P^o$ ground state. The current BSR-690 and BSR-39 results are compared with model-potential (MP) calculations [1].

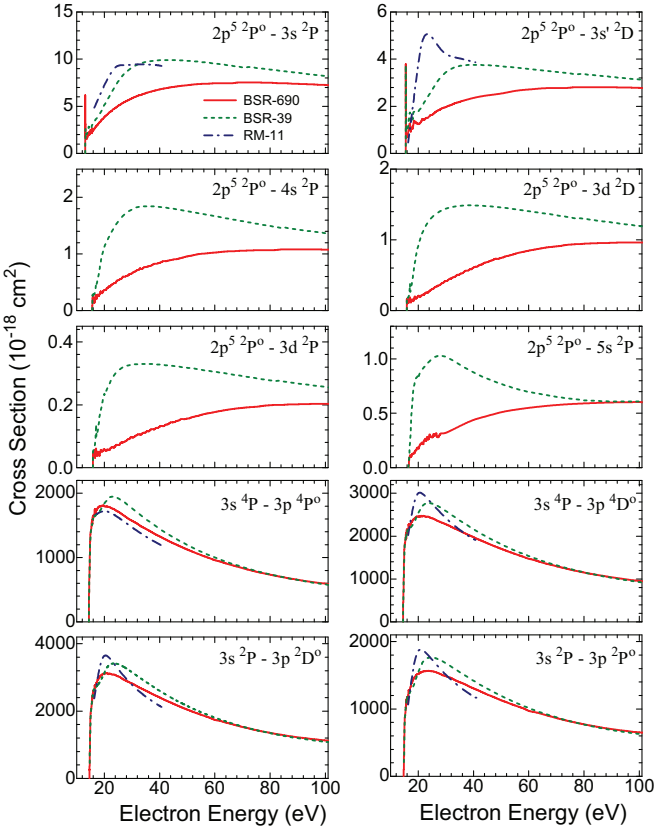

FIG. 2. (Color online) Cross sections as a function of collision energy for the most important dipole transitions in fluorine. The current BSR-690 results are compared with those from a BSR-39 model and an 11-state *R*-matrix (RM-11) calculation [5]. The prime in the notation of the $3s'\,^2D$ state indicates a $(2p^4)^1D$ core.

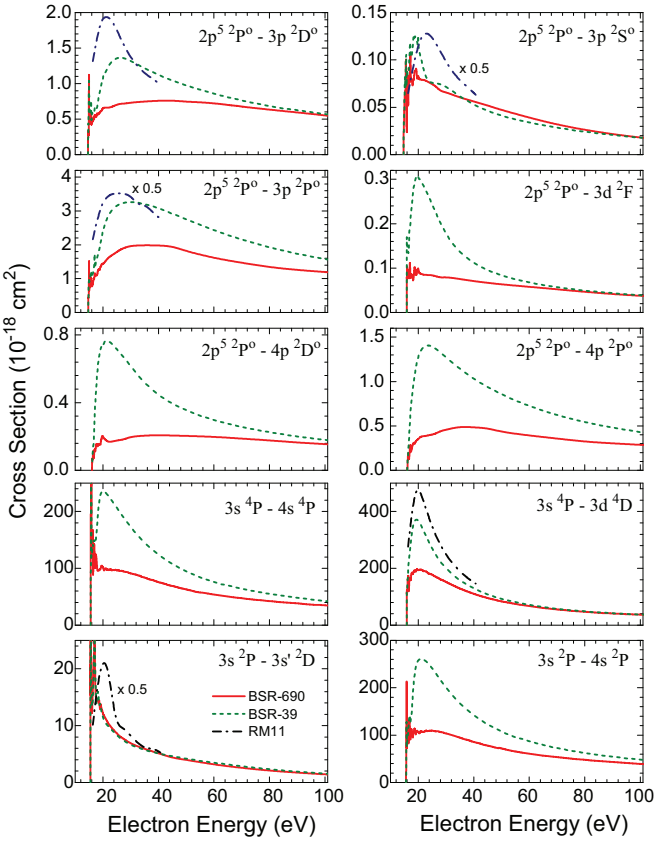

FIG. 3. (Color online) Cross sections as a function of collision energy for the most important nondipole transitions in fluorine. The current BSR-690 results are compared with those from a BSR-39 model and an 11-state *R*-matrix (RM-11) calculation [5]. The prime in the notation of the $3s'\,^2D$ state indicates a $(2p^4)^1D$ core.

continuum pseudostates. This allows us to check, at least to some extent, the convergence of the close-coupling expansion.

As seen from Fig. 2, the inclusion of the continuum pseudostates results in a significant reduction of the predicted cross sections at low and intermediate electron energies for transitions from the $2p^5$ ground states. The most pronounced effect occurs for the $2p \rightarrow 3d$ excitation. This is very similar to our findings for electron-impact excitation of Ne [22] with the $2p^6$ ground state and Ar [23] with $3p^6$. For transitions between excited states, on the other hand, involving only the excitation of a single outer electron, the influence of the continuum pseudostates is much less important. However, this is not a common rule for all one-electron transitions, as we will see below for the nondipole transitions. Dipole transitions between excited states are typically very strong in comparison to the corresponding transitions from the ground state, and hence corrections from channel-coupling effects are expected to be much smaller.

The only previous results available for comparison are those from an 11-state *R*-matrix calculation (RM11) by Baliyan and Bhatia [5]. They provide collision strengths for incident energies up to 40 eV. Comparison with the RM11 calculations shows reasonably good agreement with our BSR-39 results for the resonant $(2p^5)^2P^o$–$[2p^4(^3P)3s]^2P$ transition and for one-electron transitions between excited states. A major difference, however, is found for the $(2p^5)^2P^o$–$[2p^4(^1D)3s]^2D$ transition. The reason for this discrepancy is not completely clear, but we believe that it is related to the different configuration expansions for this state in the RM11 and our BSR calculations. Recall that we employ term-dependent orbitals, whereas in the standard RM11 calculations the $3s$ orbital, for example, is the same for the entire $2p^4(L'S')3s$ manifold with different parent terms.

The strong influence of continuum pseudostates is also found for nondipole transitions presented in Fig. 3. Here large corrections due to continuum coupling are seen for transitions from the ground state as well as for transitions between excited states. These transitions are relatively weak, and hence close-coupling effects are expected to be much more important in these cases. The exception is the strongly forbidden $3s\,^2P$–$3s'\,^2D$ transition, which occurs mainly due to exchange and should be considered separately. For nondipole transitions, the agreement with the RM11 results is much worse than for the dipole transitions considered above. In this case, even the BSR-39 cross sections agree with the RM11 results only within a factor of 2.

The exchange transitions shown in Fig. 4 exhibit qualitatively the same agreement between the different models as the dipole transitions. The corrections due to coupling to the target continuum are larger for excitation from the ground state. Here

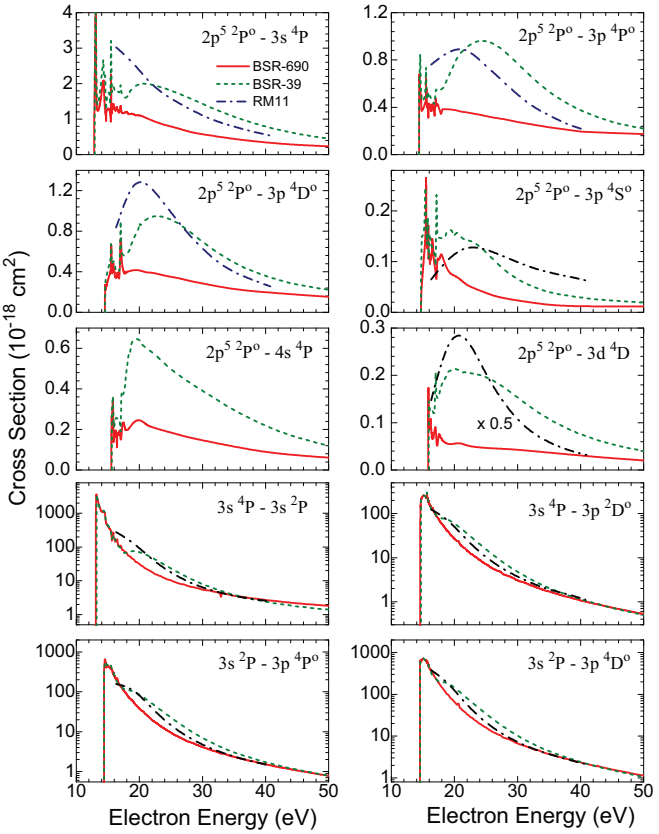

FIG. 4. (Color online) Cross sections as a function of collision energy for the most important exchange transitions in fluorine. The current BSR-690 results are compared with those from a BSR-39 model and an 11-state R-matrix (RM-11) calculation [5].

the cross sections exhibit wide near-threshold maxima, which are strongly suppressed at intermediate energies in the BSR-690 model. The RM11 results are in reasonable agreement with the BSR-39 predictions. Since exchange matrix elements are more sensitive to the target representation, the difference between the BSR-39 and RM11 results is most likely due to the different target wave functions. The cross sections for transitions between excited states are two to three orders of magnitude larger than those from the ground state. As a result, they are much less sensitive to channel-coupling effects, and all models provide very similar results.

Ionization cross sections are presented in Fig. 5. The BSR-690 ionization cross sections were obtained as the sum of the excitation cross section to all fluorine autoionizing states and the continuum pseudostates. We assumed that the radiative decay of the autoionizing states is negligible in comparison to the autoionization channel. The BSR-690 results agree closely with the measurements [7]. Although the theoretical cross sections are systematically about 15% lower that the experimental data, they lie well within the 20% uncertainty estimate of the measurements. At higher energies the theoretical predictions quickly decrease with increasing energy. This can be explained partly by an insufficient coverage of the target continuum by the present pseudostates and partly by the opening of additional ionization or ionization-excitation channels.

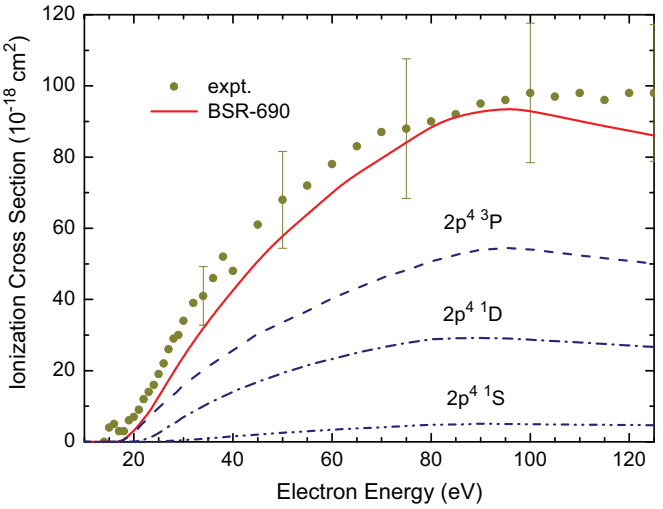

FIG. 5. (Color online) Cross section for electron-impact ionization of fluorine from the $(2s^2 2p^5)^2P^o$ ground state. The present BSR-690 results are compared with the experimental data of Hayes *et al.* [7]. Also shown are the partial cross sections for producing the $2p^4\ ^3P$, ^1D, and ^1S states of F^+.

Figure 5 also shows the cross section for individual final ionic states. These cross sections were obtained by projection of the continuum pseudostates to the given ionization channel, as described in our recent work on simultaneous ionization excitation of helium [24]. The dominant ionization channel leads to the lowest ionic state $2p^4\ ^3P$, but the ionization channel for the next ionic state, $2p^4\ ^1D$, is also important. The contributions from the ionic state $2p^4\ ^1S$ as well as from $2s$ ionization (not shown in the figure) are negligible.

Finally, Fig. 6 exhibits the grand total cross section for electron collisions with fluorine atoms in their $(2p^5)^2P^o$ ground state, i.e., the sum of angle-integrated elastic, excitation,

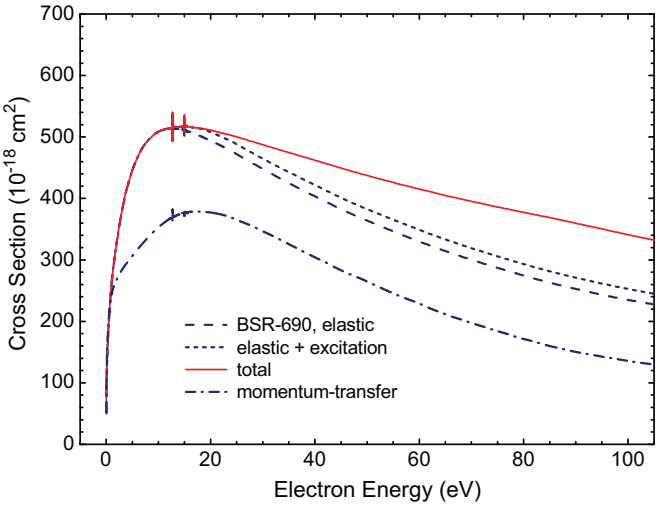

FIG. 6. (Color online) Grand total cross section for electron collisions with fluorine atoms in their $(2p^5)^2P^o$ ground state. Also shown are the contributions from elastic scattering alone and elastic scattering plus excitation processes, as well as the momentum-transfer cross section.

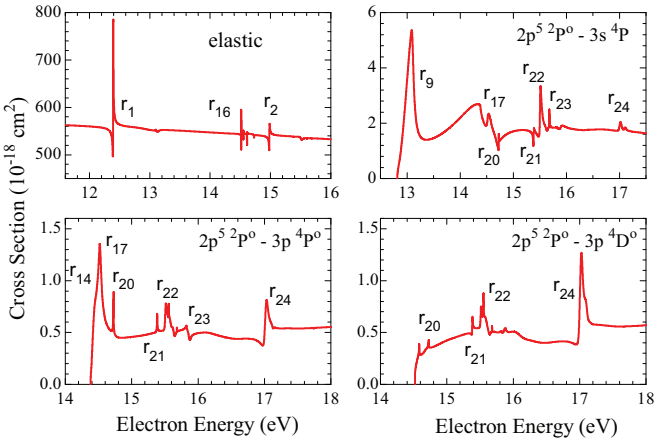

FIG. 7. (Color online) Example of resonance structure in the cross sections for selected transitions from the ground state. The cross sections were obtained with the BSR-39 model.

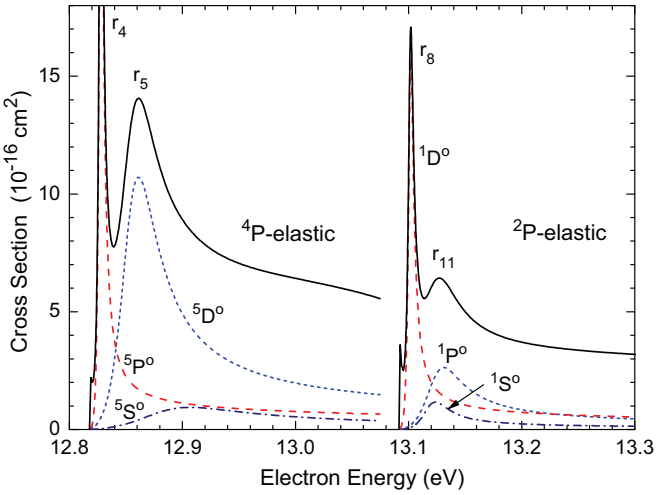

FIG. 8. (Color online) Example of a partial-wave analysis used for the classification of resonance features. The cross sections were obtained with the BSR-39 model.

and ionization cross sections. While the elastic cross section provides the largest contribution over the energy range shown, ionization gives a substantial contribution at 100 eV and higher. Overall, excitation processes represent less than 10% of the grand total cross section. Since the momentum transfer rather than the elastic cross section is typically important for plasma modeling, it is also shown in Fig. 6. The difference between the two cross sections is substantial over the entire energy range, and hence the elastic cross section is not recommended as a substitute in case the momentum-transfer result is not available.

The present calculations revealed a rich resonance structure for most electron-induced transitions in atomic fluorine at low energies. Examples of the resonance features are exhibited in Fig. 7 for a few selected transitions from the ground state. As seen from these examples, most of the resonance features are very narrow and hence the overall contribution of resonances to the corresponding rate coefficients is expected to be negligible. From a fundamental point of view, of course, it is still interesting to analyze these features. In order to classify the resonance structure, we carried out a partial-wave analysis based on the calculation of the eigenphase sum for each partial wave. An example is shown in Fig. 8. The energy regions where the eigenphase sum δ rises by π were recalculated with a small energy step of 10^{-4} eV, in order to determine the energy derivative of the eigenphase sum with high accuracy. In a resonance regime, this derivative obeys a Lorentzian form, whose maximum defines the position of the resonance while the resonance width equals $2/(d\delta/dE)$ taken at the resonance position. Note that the R-matrix method does not provide a direct recipe for classification of the resonances. In order to get some indirect clues regarding the classification, we analyzed the channel expansion of the R-matrix poles in the vicinity of the most prominent features. If appropriate, the largest contribution from the closed channels was taken as the principal component of the resonance under consideration. Table III summarizes the resonance features identified in the present calculations based on the BSR-39 model. Since the resonances occur at relatively low energies near the excitation thresholds, these results are expected to be very close to those from the BSR-690 model. The latter, however, is prohibitively time consuming for such detailed calculations.

The most prominent feature is the $2p^4(^3P)3s^2$ resonance, which manifests itself as a distinguished structure at 12.39 eV even in the large elastic cross section (cf. Fig. 1). Its position is in reasonable agreement with the value of 12.29 eV from the MCHF calculations by Clark [25]. Note that in the close-coupling calculations the resonance positions are directly related to the position of the target states. We use the

TABLE III. Resonance parameters for e–F collisions.

Index	Configuration	Term	Energy (eV)	Width (meV)
1	$2p^4(^3P)3s^2$	^3P	12.394	5.1
2	$2p^4(^1D)3s^2$	^1D	14.982	6.8
3	$2p^4(^1S)3s^2$	^1S	17.933	23
4	$2p^4(^3P)3s(^4P)3p$	$^5P^o$	12.828	4.4
5		$^5D^o$	12.855	35
6		$^5S^o$	12.880	92
7		$^3P^o$	12.946	215
8	$2p^4(^3P)3s(^2P)3p$	$^1D^o$	13.102	5.4
9		$^3P^o$	13.103	45
10		$^3S^o$	13.106	53
11		$^1S^o$	13.120	24
12		$^1P^o$	13.124	30
13	$2p^4(^3P)3p^2$	^5D	14.392	4.4
14		^3S	14.410	82
15		^5P	14.428	26
16		^1D	14.518	0.3
17		^3P	14.523	44
18		^1P	14.552	1.0
19		^1S	14.611	1.1
20	$2p^4(^3P)3p(^4D)3d$	$^3P^o$	14.731	4.0
21	$2p^4(^3P)4s^2$	^3P	15.384	8.6
22	$2p^4(^1D)3s(^2D)3p$	$^3P^o$	15.509	22
23	$2p^4(^1D)3s(^2D)3p$	$^3F^o$	15.514	12
24	$2p^4(^1D)3p^2(^3P)$	^3D	17.017	42

theoretical target energies, and the errors in the target energies affect the position of resonances.

The only experimental evidence of negative-ion resonances in F^- was obtained by Edwards and Cunningham [26]. They measured ejected electron spectra in collisions of F^- with He and observed a number of peaks. The peak at 14.85 ± 0.04 eV was associated with an autodetachment state of F^-. This feature was classified as the F^- $2p^4(^1D)3s^2$ state, based on the agreement in energy with an unpublished calculation of Matese, Rountree, and Henry performed in a similar way as their earlier work on chlorine [27]. Our prediction for this state of 14.98 eV can be considered as additional support for this classification. The remaining $2p^4(^1S)3s^2$ state for this configuration lies at the much higher energy of 17.93 eV and does not have any noticeable influence on the excitation cross sections, most likely due to the large number of possible decay channels, including double autodetachment. Our energy is again in reasonable agreement with the MCHF calculations by Buckman and Clark [28] who list 17.69 eV for this state.

The other resonances presented in Table III are also of Feshbach type with a large variety of widths, from very narrow to very wide. Some of these resonances and the corresponding peaks are depicted in Fig. 7 according to their numbering in Table III. We are not aware of any *e*–F scattering calculations that included the study of the resonance structure.

IV. SUMMARY

We have presented an extensive set of electron scattering data for neutral fluorine, including elastic scattering, momentum transfer, excitation processes, and ionization of the ground state. State-to-state excitation cross sections were obtained for all transitions between the lowest 26 states of fluorine, while results were presented for selected transitions. The calculations were performed with a parallel version of the BSR code [8], in which a *B*-spline basis is employed to represent the continuum functions inside the *R*-matrix sphere. Another distinguishing feature of the BSR calculations is the use of nonorthogonal orbitals, both in constructing the target wave functions and in representing the scattering functions. This technique allows us to generate an accurate target description and minimize pseudoresonance structure at higher energies.

Given the lack of available experimental and theoretical data, it is crucial that theoretical predictions are validated in some way. Our most extensive calculations include 690 target states. In order to check such important effects as target polarization and excitation to the target continuum, we compared the results with those from a model that only included bound states. Significant differences between the results from these models indicate a slow convergence of the close-coupling expansion in the *e*–F scattering problem. It seems highly desirable to have independent experimental data as well as results from other calculations in order to establish a reliable database of the excitation cross sections.

The present calculations were motivated, in part, to check the very strong effect of the target continuum on the excitation cross sections at intermediate scattering energies that we found earlier for several atoms. In particular, a very strong influence of coupling to the target continuum was found for *e*–Ne [22] and *e*–Ar [23] collisions, and to a lesser extent also for *e*–C [29] and *e*–Si [30]. This extreme sensitivity seems to be a general trend for atoms with outer *p* shells, closed or open, where the effect is much more substantial than for excitation of atoms with outer *s* shells, which were the subject of numerous earlier applications of the *R* matrix with pseudostates method. Note that the continuum pseudospectrum of atoms with outer *p* shells is much more dense and hence requires significantly larger computational efforts on supercomputers.

Electronic files with the current results, for electron energies up to 100 eV, are available from the authors upon request.

ACKNOWLEDGMENTS

This work was supported by the United States National Science Foundation under Grants No. PHY-0903818 and No. PHY-1212450, and by the XSEDE supercomputer allocation No. PHY-090031. The calculations were carried out on Stampede at the Texas Advanced Computing Center and on Gordon at the San Diego Supercomputer Center.

[1] E. J. Robinson and S. Geltman, Phys. Rev. **153**, 4 (1967).
[2] S. Ormonde, Phys. Rev. Lett. **38**, 690 (1977).
[3] W. D. Robb and R. J. W. Henry, Phys. Rev. A **16**, 2491 (1977).
[4] T. N. Rescigno, A. U. Hazi, and N. Winter, Phys. Rev. A **16**, 2488 (1977).
[5] K. S. Baliyan and A. K. Bhatia, Phys. Rev. A **50**, 2981 (1994).
[6] P. G. Burke, *R-Matrix Theory of Atomic Collisions* (Springer-Verlag, Berlin, Heidelberg, 2011).
[7] T. R. Hayes, R. C. Wetzel, and R. S. Freund, Phys. Rev. A **35**, 578 (1987).
[8] O. Zatsarinny, Comput. Phys. Commun. **174**, 273 (2006).
[9] O. Zatsarinny and K. Bartschat, Phys. Rev. A **77**, 062701 (2008).
[10] O. Zatsarinny and K. Bartschat, J. Phys. B **46**, 112001 (2013).
[11] O. Zatsarinny and S. S. Tayal, J. Phys. B **35**, 241 (2002).
[12] O. Zatsarinny and S. S. Tayal, J. Phys. B **34**, 3383 (2001).
[13] Y. Wang, O. Zatsarinny, K. Bartschat, and J.-P. Booth, Phys. Rev. A **87**, 022703 (2013).
[14] O. Zatsarinny and C. Froese Fischer, Comput. Phys. Commun. **180**, 2041 (2009).
[15] C. Froese Fischer, Comput. Phys. Commun. **176**, 559 (2007).
[16] http://physics.nist.gov/cgi-bin/AtData.
[17] C. Froese Fischer and G. Tachiev, At. Data Nucl. Data Tables **87**, 1 (2004).
[18] S. S. Tayal and O. Zatsarinny, Phys. Rev. A **78**, 012713 (2008).
[19] T. W. Gorczyca and N. R. Badnell, J. Phys. B **30**, 3897 (1997).
[20] C. Blondel, P. Cacciani, C. Delsart, and R. Trainham, Phys. Rev. A **40**, 3698 (1989).
[21] N. Badnell, J. Phys. B **32**, 5583 (1999); see also http://amdpp.phys.strath.ac.uk/UK_RmaX/codes.html
[22] O. Zatsarinny and K. Bartschat, Phys. Rev. A **86**, 022717 (2012).

[23] O. Zatsarinny, Y. Wang, and K. Bartschat, Phys. Rev. A **89**, 022706 (2014).
[24] O. Zatsarinny and K. Bartschat, J. Phys. B **47**, 061001 (2014).
[25] C. W. Clark, in *Advances in Laser Science – I*, edited by W. C. Stwalley and M. Lapp (American Institute of Physics, New York, 1986), p. 379.
[26] A. K. Edwards and D. L. Cunningham, Phys. Rev. A **9**, 1011 (1974).
[27] J. J. Matese, S. P. Rountree, and R. W. Henry, Phys. Rev. A **8**, 2965 (1973).
[28] S. J. Buckman and C. W. Clark, Rev. Mod. Phys. **66**, 539 (1994).
[29] Y. Wang, O. Zatsarinny, and K. Bartschat, Phys. Rev. A **87**, 012704 (2013).
[30] V. Gedeon, S. Gedeon, V. Lazur, E. Nagy, O. Zatsarinny, and K. Bartschat, Phys. Rev. A **85**, 022711 (2012).